01

Effect of the Dislocation Dipoles with Different Arms on the Graphene Deformation Behavior: molecular dynamics

© A.Kh. Akhunova[1,2], Yu.A. Baimova[1,2]

[1]Institute of Metal Superplasticity Problems, Russian Academy of Sciences,
Ufa, Bashkortostan, Russia
[2]Ufa University of Science and Technology,
Ufa, Russia
e-mail: akhunova.a.a@gmail.com

Received January 16, 2023
Revised January 16, 2023
Accepted January 16, 2023

The molecular dynamics simulation is used to analyze the features of the deformation behavior and the process of fracture of graphene with dislocation dipoles with different arm. Moreover, the wrinkling of graphene during deformation is taken into account, which greatly reduces the strength of graphene. It has been established that an increase in temperature slightly affects the mechanical properties of graphene with dislocation dipoles, in contrast to defect-free graphene and graphene with a Stone–Wales defect. It is shown that a change in the distance between dislocations in a dipole does not significantly affect the elastic modulus and graphene strength. However, the presence of dislocation dipoles can affect graphene wrinkling during stretching.

Keywords: graphene, dislocation dipole, mechanical properties, molecular dynamics.

DOI: 10.21883/TP.2023.04.55930.6-23

Introduction

Defects in the crystal structure naturally appear in graphene during its synthesis, which is especially typical for its large-scale production. Defects can also appear b of external influences in local areas of stress concentration both during graphene synthesis and at high temperatures [1–4]. The presence of defects in the crystal lattice can significantly affect the mechanical [3–7], chemical [8], electronic and transport [9–11] properties of graphene.

One of the most common defects is the Stone−Wales (SW) defect, which is formed due to the rotation of the C−C bond in the plane of the graphene sheet with the transformation of four neighboring hexagons into two pentagons and two heptagons [1,12,13]. A SW defect can be also considered as a dislocation dipole (DD), in which two edge dislocations with opposite signs of the Burgers vector are shifted by one lattice period [14,15]. This pair of dislocations can also be separated by some distance, called the dipole arm. As a rule, the presence of DD leads to wrinkling of graphene [14,16,17]. The strength of defect-free graphene is very high; however, real graphene contains structural defects that worsen its mechanical properties [3–7,18–20]. For example, the fracture toughness of defective graphene depends on temperature and strain rate [21]. It has been found that an increase in temperature reduces the mechanical properties of both defect-free and defective graphene [22]. In Ref. [23], the influence of defects and doping on the mechanical properties of graphene was studied and it was found that the location of defects and their concentration are important factors in determining its mechanical properties. The strength of graphene is very important for the future development of high-performance graphene materials and devices from various fields, in particular, in the creation of flexible ultrathin displays.

Another important problem that still remains relevant is the stability of graphene. Landau, Peierls, and Mermin [24–26] discussed the instability of two-dimensional ($2D$) structures. According to the Mermin−Wagner theorem [26], long-wavelength fluctuations destroy the long-range order in two-dimensional crystals. However, the stability of a $2D$ material is achieved due to the formation of wrinkles [27]. Indeed, single-layer graphene can spontaneously form wrinkles caused by the temperature factor [28–30]. Wrinkling caused by defects has also been observed in other studies [31,32].

The effect of wrinkles on the properties of graphene is a nontrivial issue. It has been shown that even initially flat graphene can wrinkle under applied deformation [33,34]. Such wrinkling of graphene reduces its elastic moduli and changes Poisson's ratio [35,36]. However, on the other hand, graphene with monotonically distributed wrinkles demonstrates high strength [35]. Interestingly, corrugated graphene can even be used to increase the strength of metal composites [37,38].

In this paper, the deformation behavior of graphene containing dislocation dipoles of different lengths at zero and room temperatures is studied using the molecular dynamics method. The purpose of this work was to study how the presence of defects and wrinkles affects the process of stretching and fracture of graphene.

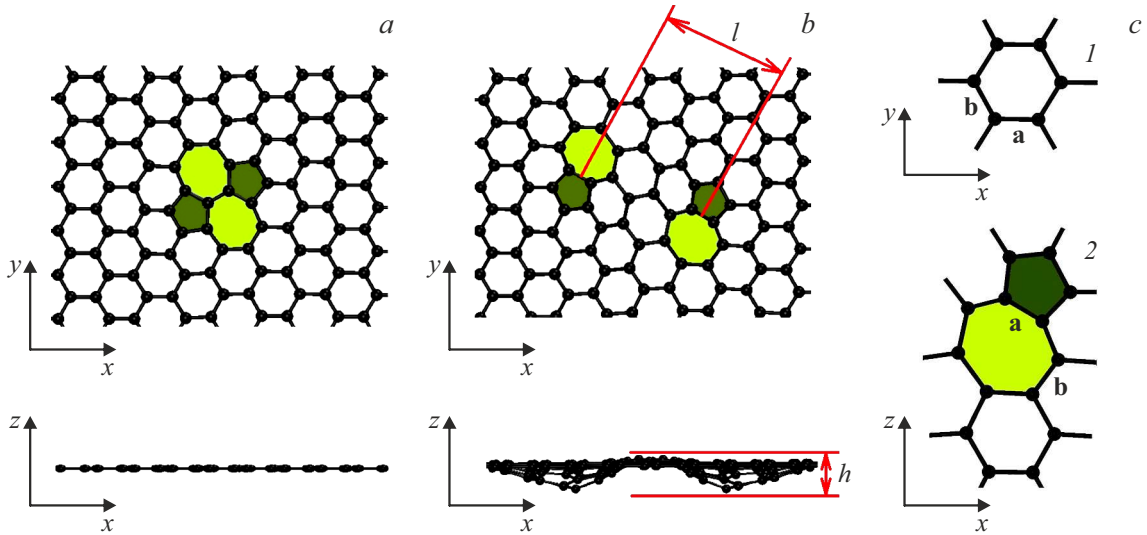

Figure 1. Fragment of a graphene cell in two projections: *a* — graphene with a SW defect, *b* — graphene with DD_2. Here *l* is the distance between two dislocations, called the dipole arm, *h* is the height of the bubble formed by the defect. The geometric parameters of all considered DDs are given in the text; *c* — notation of bonds in defect-free (*1*) and defective graphene (*2*): *a* — denotes the bond in the armchair direction, *b* — in the zigzag direction.

1. Technique of studies

A calculation cell of graphene with a size of 74×103 Å in two-dimensional space (x, y) was considered. To prevent the interaction of graphene with its own periodic images, the cell size along the z axis was set equal to 200 Å. In total, the cell contained 31 000 carbon atoms. For each structure, before stretching, the energy of the system was minimized. Strain fields in graphene caused by the presence of dislocations lead to its warping [39], however, in this work, periodic boundary conditions applied along the x and y directions suppressed it. Thus, graphene was in the stability region (in a planar configuration), and perturbations induced by DD caused the formation of a bubble in the region of each dislocation, which is in good agreement with Refs. [40,41], in which the formation and evolution of dislocation pairs separated by different distances were studied using the methods of molecular dynamics and density functional theory (DFT) analysis.

A dislocation dipole consists of two dislocations (5–7 defect) separated by a distance, which is defined as the dipole arm l, as shown in Fig. 1. The height h of the bubble top relative to the graphene plane non-monotonically changes as the distance between dislocations increases. In this problem, the dipole orientation angle is equal to $\pi/6$, although it can vary over a wide range [42]. The well-known SW defect can be considered as a zero-shoulder DD [42]. The Burgers vector B for the dislocations that make up the DD is defined as $B = \sqrt{3}a$, where $a = 1.42$ Åis the C–C bond length in graphene. Below structures with DD will be denoted as DD_n, where the subscript n indicates the distance between two pairs of dislocations in the number of hexagons separating them. As an example, Fig. 1 shows fragments of cells with a SW defect and with DD_2.

6 kinds of DDs were considered: SW (with zero arm $l = 0$ Å and height $h = 0$ Å); DD_2 (with arm $l = 6$ Å and height $h = 1.89$ Å); DD_4 ($l = 11$ Å, $h = 2$ Å); DD_6 ($l = 15$ Å, $h = 1.25$ Å); DD_8 ($l = 20$ Å, $h = 1.22$ Å); DD_{10} ($l = 25$ Å, $h = 1.78$ Å).

Note that the bubble height depends non-monotonically on the arm length. This can be explained by the high nonlinearity of the phenomenon of graphene wrinkling, which is affected not only by the initial sample geometry, the type, number [41,43] and orientation angle of dipoles, but also by the used periodic boundary conditions [44]. In the future, it is reasonable to study the influence of various periodic boundary conditions on the process of bubble formation on defects.

Graphene structures with defects were obtained using original software packages. Simulation of uniaxial tension in the directions of the x-axis (armchair) and y-axis (zigzag) was carried out using the LAMMPS software package. The interaction between carbon atoms was described by the AIREBO potential [45].

Uniaxial tension was carried out at a constant strain rate of $0.005\,\text{ps}^{-1}$ under isothermal conditions at temperatures of 0 and 300 K. The temperature during the simulation was controlled by a Nose–Hoover thermostat using an nvt ensemble. The simulation results obtained at 300 K were averaged over at least 50 tests at given strain values. The moment of graphene fracture was determined according to two criteria: bond breaking and a sharp decrease in the potential energy of the system. These two criteria give a close value of the critical rupture time.

Tensile strength σ_{UTS}, fracture strain ε_F and elastic modulus E of graphene as a function of dipole arm l during tensile tests in the armchair (a) and zigzag (z) direction

Temperature, K	l, Å	σ^a_{UTS}, GPa	σ^z_{UTS}, GPa	ε^a_F	ε^z_F	E^a, GPa	E^z, GPa
0	Graphene	8.14	7.11	0.51	0.43	16.43	13.94
	0	5.67	6.33	0.49	0.42	16.36	13.86
	6	1.56	1.48	0.49	0.41	4.14	3.29
	11	1.27	1.32	0.49	0.42	3.76	3.00
	15	1.20	1.47	0.49	0.41	3.87	3.45
	20	1.07	1.43	0.49	0.41	3.76	3.34
	25	1.24	1.45	0.49	0.4	3.95	3.52
300	Graphene	3.02	6.50	0.26	0.41	15.83	13.64
	0	2.96	4.90	0.26	0.38	15.82	13.53
	6	0.74	0.93	0.23	0.34	3.97	3.57
	11	0.67	0.83	0.26	0.34	3.41	3.11
	15	0.69	1.06	0.24	0.37	3.73	3.42
	20	0.68	0.98	0.24	0.36	3.53	3.34
	25	0.72	1.02	0.24	0.36	3.69	3.34

2. Simulation results

2.1. Tensile strength

For simplicity, the values obtained by stretching in the zigzag direction will be denoted by the superscript z, and in the armchair direction — by the superscript a. All critical values such as tensile strength σ_{UT}, fracture strain ε_F, and elastic modulus for all considered structures are given in Table.

It is known from the literature that the strength of graphene is very high, about 100 GPa [20,46–48]. However, the results obtained using numerical methods largely depend on the modeling technique [20]. For example, it was shown [49] that, under dynamic loading, covalent networks exhibit brittle fracture instead of plastic fracture due to insufficient structural relaxation. Tension of composites based on a graphene network leads to another scenario [50]: the ultimate strength of covalent systems under dynamic loading can be overestimated.

In the present work, the conditions of the problem allow warping of graphene in order to study the effect of natural folding on the fracture resistance. It is known that the strain energy in free graphene can be easily released due to the formation of wrinkles [32]. This agrees with [33,34], where it was shown that, at positive strains in one direction and negative strains in the perpendicular direction, graphene loses its stability and wrinkles of various orientations appear. In the present work, when graphene is stretched in one direction, it can be simultaneously compressed in the direction normal to the stretching axis. This leads to the formation of positive stresses in graphene along the tension axis and negative stresses along the compression axis. This fact is known and is in good agreement with the literature data. It should also be noted that the type of wrinkles significantly affects the elastic modulus and fracture resistance [35,36]: in the presence of low-amplitude graphene warping, the fracture strain and elastic modulus are lower than in planar graphene, but not as much as in graphene with high-amplitude wrinkles.

Wrinkles and folds can significantly reduce the amount of stress created by defects [39]. Thus, such low values of $\sigma^a_{UTS} = 8.1$ GPa ($\sigma^z_{UTS} = 7.1$ GPa) and high values $\varepsilon^a_F = 0.51$ ($\varepsilon^z_F = 0.43$), presented in Table 1, can be easily explained. In this case, for graphene the fracture strain upon the tension in the zigzag direction is higher than in the armchair direction ($\varepsilon^z_F > \varepsilon^a_F$). This is explained by the structural changes that occur in graphene under given stretching conditions, which will be shown below. The modulus of elasticity E was determined from the slope of the linear sections of the stress–strain curves. Here, it is assumed that elastic deformation takes place before the appearance of the first wrinkles with an amplitude above 0.5 Å.

Based on the simulation results, it was found that the stress–strain curves for graphene and graphene with a SW defect approximately coincide up to the fracture point. The same behavior of graphene with an SW defect was shown earlier [51,52]. The slope of the rectilinear part of the curves for the armchair direction is higher than for the zigzag direction, which corresponds to different moduli of elasticity (Table 1). For example, for graphene $E^a = 16.4$ GPa and $E^z = 13.9$ GPa.

Temperature also plays an important role in reducing the strength of graphene, regardless of the presence of a defect [53–55]. Thermal fluctuations cause the formation of vacancies or dislocations as the temperature increases the possibility of atomic movement in the structure. As a result, the strength of graphene becomes significantly reduced. The tensile strength and fracture strain of graphene under tension along the armchair direction at room temperature decreases by more than two times, compared with the calculation at 0 K (see Table). Similar results were obtained for graphene with an SW defect. The elastic modulus E is

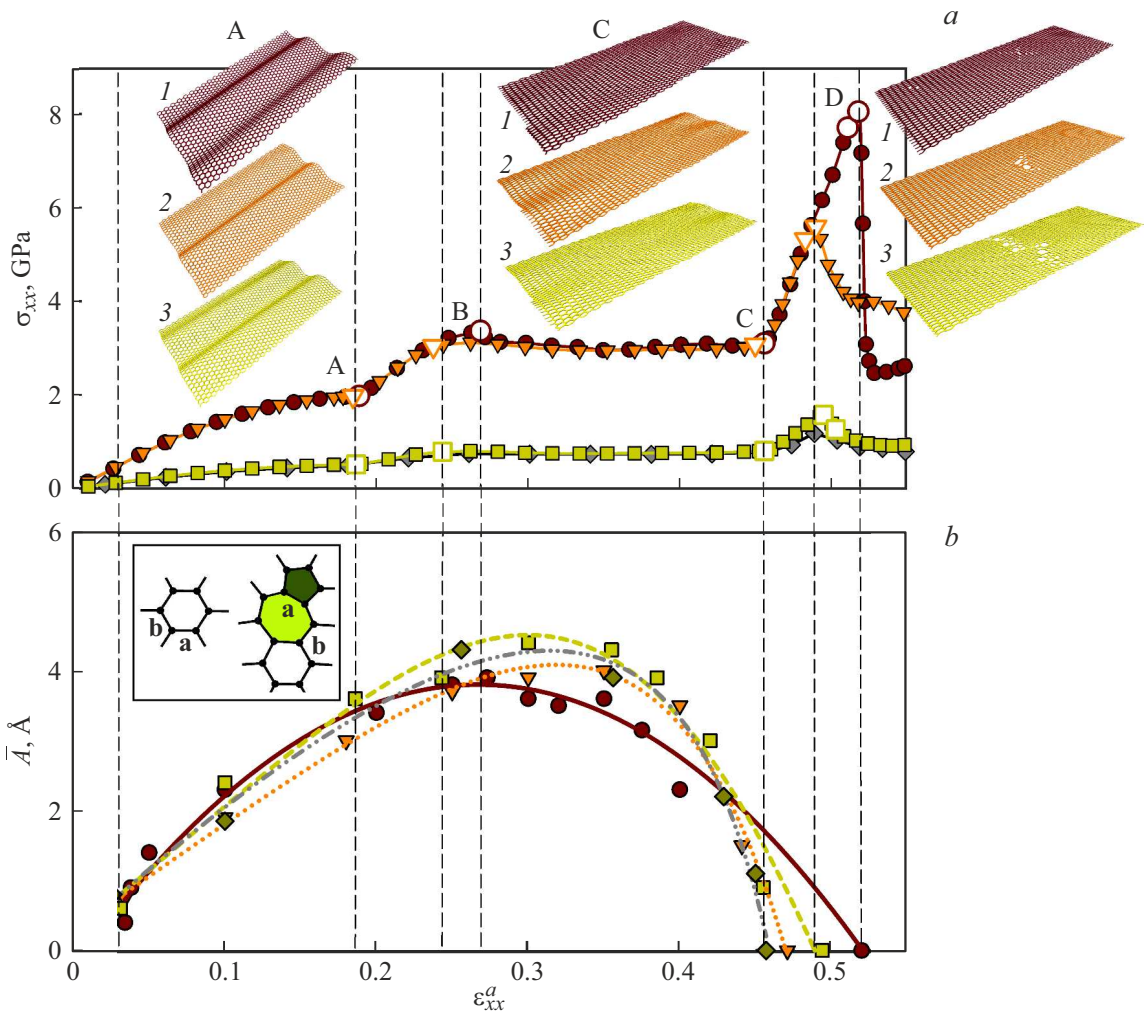

Figure 2. Results of stretching simulation along the armchair direction at $T = 0$ K. Vertical thin black dashed lines show different stages of deformation. *a* — dependence of stress on strain for graphene (circles), graphene with SW defect (triangles), DD_2 (squares) and DD_6 (diamonds). Points A, B, C, D denote the transition from one stage of loading to another for each structure. The structure at critical points A, C and at the moment of destruction is given in axonometric projection: graphene (*1*), graphene with SW (*2*) and graphene with DD_2 (*3*); *b* — average wrinkle amplitude $\bar{A}$ as a function of the degree of deformation for defect-free graphene (circles), graphene with SW (triangles), DD_2 (squares) and DD_6 (diamonds). Symbols show numerical data, lines — their approximation. There is also an illustration of the notation of bonds in defect-free and defective graphene: *a* — bond in the armchair direction, *b* — in the zigzag direction.

practically independent of temperature, which is consistent with previous studies [56]. An increase in temperature significantly reduces of σ^a_{UTS} graphene and graphene with a SW defect, while for graphene with DD, the temperature has almost no effect on σ^a_{UTS}. When stretching in the zigzag direction, the effect of temperature is not so significant.

The very close slope angles of the linear sections of the stress–strain curves for all structures with DD show that the distance between dislocations in a dipole does not significantly affect the elasticity modulus of graphene. The found values of E are in the range from 3.76 to 4.14 GPa for stretching along the „armchair" direction, and from 3.00 to 3.52 GPa for stretching along the „zigzag" direction. Hence, we can conclude that the presence of DDs does not significantly affect the elastic properties of graphene. Previously, in experimental and theoretical studies, it was shown that the elastic properties are similarly independent of the type of grain boundary [7,57].

2.2. Analysis of fracture mechanisms

The appearance of wrinkles under given deformation conditions determines the form of stress–strain curves. Figure 2, 3 shows the dependences of the stress (Fig. 2, *a*, 3, *a*) and the average wrinkle amplitude (Fig. 2, *b*, 3, *b*) on the degree of strain for stretching along the armchair(zigzag) direction at a temperature of 0 K for graphene, SW, DD_2 and DD_6. Dependences are presented only for DD_2 and DD_6, since the general behavior of graphene is almost the same. All revealed differences will be discussed in the text. The

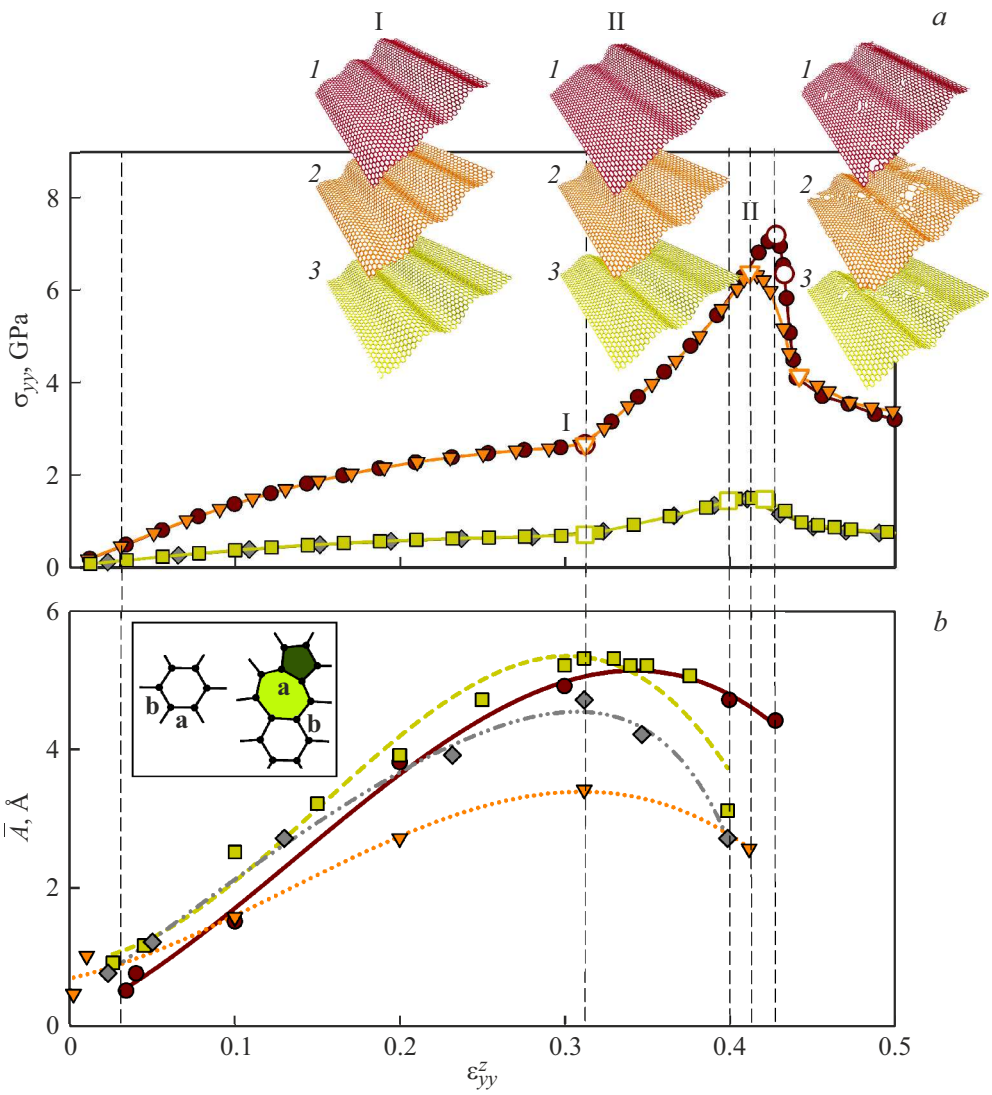

Figure 3. Results of stretching simulation along the armchair direction at $T = 0$ K. Vertical thin black dashed lines show different stages of deformation. *a* — dependence of stress on strain for graphene (circles), graphene with SW defect (triangles), DD_2 (squares) and DD_6 (diamonds). Points I and II denote the transition from one stage of loading to another for each structure. The structure at critical points I, II and at the moment of destruction is given in axonometric projection: graphene (1), graphene with SW (2), and graphene with DD_2 (*3*); *b* — average wrinkle amplitude $\bar{A}$ as a function of the degree of deformation for defect-free graphene (circles), graphene with SW (triangles), DD_2 (squares) and DD_6 (diamonds). Symbols show numerical data, lines — their approximation. There is also an illustration of the notation of bonds in defect-free and defective graphene: *a* — bond in the armchair direction, *b* — in the zigzag direction.

evolution of the structure of the considered DDs at critical points is also presented.

The mean amplitude of wrinkles is calculated as $\bar{A} = 0.5(|A_{\max}| + |A_{\min}|)$, where $A_{\max}$ is the maximum amplitude and $A_{\min}$ is the minimum amplitude of the wrinkles. The obtained value of the amplitudes is in good agreement with the literature data [30,32]. The form of dependences of the average amplitude on the degree of deformation for DD_2 and DD_6 defects shows that graphene with any DD forms wrinkles of nearly the same amplitude.

Consider in more detail the tensile strain curves in the armchair direction. Since the curves for DD_2 and DD_6 are almost identical, we will only consider DD_2 below. Four stages of loading can be distinguished on the deformation curves: I — after the end of the elastic stage and up to point A; II — between A and B; III — between B and C; IV — between C and D. Practically for all structures, the same nature of deformation is observed at critical points. Point C can be considered as a precritical state. Note that at point D for defect-free graphene, the level of critical stress is higher than for defective structures.

Before point A, the amplitude of the wrinkles gradually increases for all structures. It should be noted that the cell size of the structure in the x direction (armchair) is large enough to obtain two wrinkles with the same parameters. Previously, in Ref. [32], it was shown that the amplitude

and length of a wrinkle depend on the size of the graphene nanoribbon, which is also true for graphene sheet. The maximum value of the wrinkle amplitude for graphene is reached at point B, for graphene with SW and DD_2 — at $\varepsilon^a_{xx} = 0.3$. Note that the deformation occurs due to two factors: a change in the lattice parameter and a change in the amplitude of the graphene wrinkles.

Let us analyze the transformation of bonds in the structure upon the stretching of graphene and graphene with defects. For simplicity, let us denote the bonds in the armchair direction by a, in the zigzag direction by b b (Figs. 2 b, 3 b). With the beginning of the deformation in graphene, the bond a continuously stretches up to point A, reaching a length of 1.7 Å, which remains constant up to the point C. The length of bond $b$begins to grow only after point A. Since after point A the bond can no more elongate, further deformation occurs at the expense of increasing the amplitude of the wrinkles, change of valence angles and the length of bond b. After point C, the bond begins to elongate again up to rupture. Figure 2 shows that at point C the graphene flattens, so that the stretching of bonds is the dominant deformation mechanism.

If we consider structures with DD_n, then the main changes in bond lengths occur near the defect, and not directly on it. The bond a (common for the pentagon and heptagon that make up the dislocation) behaves similarly to the bond a in graphene and is the strongest. The rest of the bonds in the defect and near it practically do not change up to point B. Then there is a rapid increase in the b bond length, which makes further stretching of the graphene possible. Thus, it can be concluded that when the bonds are oriented along the direction of stretch (in this case armchair), they can provide stretch with simultaneous wrinkling. However, when these bonds are critically strained, bonds with a different orientation begin to play the main role.

Note that the location of the defect affects the distribution of wrinkles. Upon deformation, the SW defect is located on the wall of one of the wrinkles, while DD_2 finds itself between two wrinkles. An increase in the dipole arm leads to a slight redistribution in the structure: each dislocation in the dipole is located on the walls of opposite wrinkles. After the transition from wavy to flat graphene, for all the structures considered, one more structural transformation occurs at point C: hexagons with the equal length of bonds are transformed into elongated ones, and this is a subcritical transformation. In defect-free graphene, fracture can begin at an arbitrary point in its basis plane. For graphene with DD, the flattening of the wrinkles starts from the location of the defect, and then, after the complete flattening of the graphene, its fracture occurs starting close to the defect and running diagonally from the heptagon.

It should be noted that graphene with DD_6 shows a tendency to the appearance of a third wrinkle, but the presence of a defect prevents this. Moreover, graphene with DD_6-DD_{10} do not become completely flat before fracture. Also, when these structures are stretched, a new 5−8−5 defect appears.

When stretching along the zigzag direction, the situation is somewhat simpler: only two stages are distinguished, namely, after the end of the elastic stage and before point I, and between point I and point II. The wrinkles do not disappear until destruction, while they are not uniform, unlike stretching in the armchair direction. This is because the length of the structure is not sufficient to obtain uniform wrinkles Graphene has three wrinkles at point I and two wrinkles at point II, in both cases of different amplitude. However, the presence of defects affects the configuration of the wrinkles: for graphene with SW and DD, more uniform wrinkles with similar amplitudes are formed. Similar to the case of stretching in the armchair direction, the amplitude values increase continuously up to point I, and then slowly decrease towards point II.

Let us analyze the transformation of bonds in the structure. For defect-free graphene, bond b, oriented almost in the same direction as the direction of stretching, is weaker and rapidly elongates to point I. After that, all changes in bonds and bond angles lead to a continuous increase in both bonds, a and b, until subcritical stage. For graphene with DD, at the first stage of deformation (even at $\varepsilon^z_{yy} = 0.11$), there is a sharp elongation of the bond b, which is located near the defect. The bonds along which tensile strain has been applied are the weakest bonds in graphene. When graphene with DD is stretched, the fracture begins near the defect.

Conclusion

Thus, the effect of a dislocation dipole on the strength of graphene is studied using atomistic simulation. The mechanical properties of graphene under tension along the armchair and zigzag directions at 0 and 300 K are analyzed. In this case, the case of tension is considered, in which the natural warping of graphene is allowed.

In the presence of wrinkles in graphene, the fracture process is rather complicated and includes the formation of wrinkles at the initial stage of deformation and the return to a flat shape at the later stages of stretching. In this case, continuous and rather diverse changes in bond lengths occur, as well as the appearance of new defects. All these mechanisms do not contradict each other, but act simultaneously, which leads to a sufficiently high fracture strain. However, the tensile strength and Young's modulus of wrinkled graphene are very low because wrinkling makes the graphene much weaker.

Temperature, graphene wrinkling, and the presence of defects are the main factors affecting the mechanical properties of graphene. The presence of a dislocation dipole with an arm of more than 15 Å can affect the special distribution of wrinkles, e.g., prevent their formation. An increase in the length of the dipole arm does not lead to a significant decrease in the tensile strength of graphene.

For graphene with a dislocation dipole, an increase in temperature does not lead to a significant decrease in the strength of graphene.

Funding

The research was funded within the State Assignment of IMSP RAS (Young scientist laboratory).

Conflict of interest

The authors declare that they have no conflict of interest.

References

[1] J.B. Wu, M.L. Lin, X. Cong, H.N. Liu, P.H. Tan. Chem. Society Rev., **47**, 1822 (2018). DOI: 10.1039/c6cs00915h
[2] P.M. Tailor, R.J. Wheatley, N.A. Besley. Carbon, **113**, 299 (2017). DOI:10.1016/j.carbon.2016.11.059
[3] M. Braun, F. Arca, M. Ariza. Intern. J. Mechan. Sci., **209**, 106702 (2021). DOI: 10.1016/j.ijmecsci.2021.106702
[4] A. Cao, B. Shen, Q. Lin, S. Chen, Z. Huang, Z. Ji, Z. Zhang. Computational Mater. Sci., **173**, 109423 (2020). DOI: 10.1016/j.commatsci.2019.109423
[5] S. Ajori, A. Ameri, R. Ansari. Superlattices and Microstructures, **142**, 106526 (2020). DOI: 10.1016/j.spmi.2020.106526
[6] Y. Fu, T. Ragab, C. Basaran. Mater. Sci., **124**, 142 (2016). DOI: 10.1016/j.commatsci.2016.07.022
[7] T.H. Liu, C.W. Pao, C.C. Chang. Carbon, **50**, 3465 (2012). DOI: 10.1016/j.carbon.2012.03.012
[8] T.A. Oliveira, P.V. Silva, V. Meunier, E.C. Girão. Carbon, **201**, 222 (2023). DOI: 10.1016/j.carbon.2022.08.079
[9] H. Wang, Y. Wang, B. Bai, X. Guo, J. Xue. Appl. Surf. Sci., **531**, 147347 (2020). DOI: 10.1016/j.apsusc.2020.147347
[10] M. Shakeri. Superlattices and Microstructures, **128**, 116 (2019). DOI: 10.1016/j.spmi.2019.01.019
[11] F. Wang, X. Xu, J. Mao. Diamond Related Mater., **109**, 108037 (2020). DOI: 10.1016/j.diamond.2020.108037
[12] A.K. Manna, S.J. Gilbert, S.R. Joshi, T. Komesu, S. Varma. Physica E, **143**, 115329 (2022). DOI: 10.1016/j.physe.2022.115329
[13] A.I. Podlivaev, L.A. Openov. FTT, **57** (4), 802 (2015). (in Russian).
[14] S.T. Skowron, I.V. Lebedeva, A.M. Popov, E. Bichoutskaia. Chem. Society Rev., **44**, 3143 (2015). DOI: 10.1039/c4cs00499j
[15] M. Ariza, M. Ortiz. J. Mechan. Phys. Solids, **58**, 710 (2010). DOI: 10.1016/j.jmps.2010.02.008
[16] Y. Yao, S. Wang, J. Bai, R. Wang. Physica E, **84**, 340 (2016). DOI: 10.1016/j.physe.2016.08.004
[17] M. Lazar. Phys. Lett. A, **377**, 423 (2013). DOI:10.1016/j.physleta.2012.12.005
[18] L. Xu, N. Wei, Y. Zheng. Nanotechnology, **24**, 505703 (2013). DOI: 10.1088/0957-4484/24/50/505703
[19] Y.X. Du, L.J. Zhou, J.G. Guo. Mater. Chem. Phys., **288**, 126412 (2022). DOI: 10.1016/j.matchemphys.2022.126412
[20] M. Torkaman-Asadi, M. Kouchakzadeh. Comput. Mater. Sci., **210**, 111457 (2022). DOI: 10.1016/j.commatsci.2022.111457
[21] M.A.N. Dewapriya, R.K.N.D. Rajapakse. J. Appl. Mechan., **81**, 081010 (2014). DOI: 10.1115/1.4027681
[22] K.K. Gupta, S. Dey. In: *Lecture Notes on Multidisciplinary Industrial Engineering*, ed. by R.G. Narayanan, S.N. Joshi, U.S. Dixit. (Springer, Singapore, 2019), p. 793. DOI: 10.1007/978-981-32-9072-3_66
[23] K.K. Gupta, T. Mukhopadhyay, A. Roy, S. Dey. J. Mater. Sci. Technol., **50**, 44 (2020). DOI: 10.1016/j.jmst.2020.03.004
[24] L.D. Landau. Phys. Z. Sowjet Union, **11**, 56 (1937).
[25] R. Peierls. Helv. Phys. Acta, **7**, 81 (1934).
[26] N.D. Mermin. Phys. Rev., **176**, 250 (1968).
[27] D. Nelson, L. Peliti. J. Physique, **48**, 1085 (1987). DOI: 10.1051/jphys:019870048070108500
[28] A. Fasolino, J.H. Los, M.I. Katsnelson. Nature Mater., **6**, 858 (2007). DOI: 10.1038/370nmat2011
[29] V.B. Shenoy, C.D. Reddy, A. Ramasubramaniam, Y.W. Zhang. Phys. Rev. Lett., **101**, 245501 (2008). DOI: 10.1103/physrevlett.101.245501
[30] S. Deng, V. Berry. Mater. Today, **19**, 197 (2016). DOI: 10.1016/j.mattod.2015.10.002
[31] C. Wang, L. Lan, Y. Liu, H. Tan. Comput. Mater. Sci., **77**, 250 (2013). DOI: 10.1016/j.commatsci.2013.04.051
[32] T. Zhang, X. Li, H. Gao. J. Mechan. Phys. Solids, **67**, 2 (2014). DOI: 10.1016/j.jmps.2014.02.005
[33] J.A. Baimova, S.V. Dmitriev, K. Zhou. Physica Status Solidi (b), **249**, 1393 (2012). DOI: 10.1002/pssb.201084224
[34] J.A. Baimova, S.V. Dmitriev, K. Zhou, A.V. Savin. Phys. Rev. B, **86**, 035427 (2012). DOI: 10.1103/physrevb.86.035427
[35] H. Qin, Y. Sun, J.Z. Liu, M. Li, Y. Liu. Nanoscale, **9**, 4135 (2017). DOI: 10.1039/c6nr07911c
[36] J.N. Grima, S. Winczewski, L. Mizzi, M.C. Grech, R. Cauchi, R. Gatt, D. Attard, K.W. Wojciechowski, J. Rybicki. Tailoring Adv. Mater., **27**, 1455 (2014). DOI: 10.1002/ 387adma.201404106
[37] S. Zhao, Y. Zhang, J. Yang, S. Kitipornchai. Carbon, **168**, 135 (2020). DOI: 10.1016/j.carbon.2020.06.054
[38] S. Zhao, Y. Zhang, J. Yang, S. Kitipornchai. J. Mater. Sci. Technol., **120**, 196 (2022). DOI: 10.1016/j.jmst.2021 392.12.042
[39] H.S. Seung, D.R. Nelson. Phys. Rev. A, **38**, 1005 (1988). DOI: 10.1103/physreva.38.1005
[40] G.-D. Lee, E. Yoon, K. He, A.W. Robertson, J.H. Warner. Nanoscale, **6**, 14836 (2014). DOI: 10.1039/c4nr04718d
[41] Y. Kawamura, Y. Ohta. Comp. Mater. Sci., **205**, 111224 (2022). DOI: 10.1016/j.commatsci.2022.111224
[421] E. Ertekin, D.C. Chrzan, M.S. Daw. Phys. Rev. B, **79**, 155421 (2009). DOI: 10.1103/physrevb.79.155421
[43] Y. Liu, B. I. Yakobson. Nano Lett., **10**, 2178 (2010).
[44] S. Chen. *Buckling and Topological Defects in Graphene and Carbon Nanotubes* (UC Berkeley Electronic Theses and Dissertations, University of California, Berkeley, 2012), https://escholarship.org/uc/item/59v245r8
[45] S.J. Stuart, A.B. Tutein, J.A. Harrison. Chem. Phys., **112**, 6472 (2000). DOI: 10.1063/1.481208
[46] C. Lee, X. Wei, J.W. Kysar, J. Hone. Science, **321**, 385 (2008). DOI: 10.1126/science.1157996
[47] G. Zhang, H. Liu, Y. Chen, H. Qin, Y. Liu. J. Mechan. Phys. Solids, **169**, 105080 (2022). DOI: 10.1016/j.jmps.2022.105080
[48] M. Chen, S. Quek, Z. Sha, C. Chiu, Q. Pei, Y. Zhang. Carbon, **85**, 135 (2015). DOI: 10.1016/j.carbon.2014.12.092
[49] K. Zhou, B. Liu. In book: *Molecular Dynamics Simulation, ed. by E. Thompson.* (Elsevier Inc., U.S., 2022), p. 129. DOI: 10.1016/b978-0-12-816419-8.00010-6

[50] K.A. Krylova, L.R. Safina, S.A. Shcherbinin, J.A. Baimova. Methodology for Materials, **15**, 4038 (2022). DOI: 10.3390/ma15114038
[51] B. Mortazavi, S. Ahzi. Carbon, **63**, 460 (2013). DOI: 10.1016/j.carbon.2013.07.017
[52] N. Jing, Q. Xue, C. Ling, M. Shan, T. Zhang, X. Zhou, Z. Jiao. RSC Advances, **2**, 9124 (2012). DOI: 10.1039/c2ra21228e
[53] A.I.C. Mihaila, T. Susi, J. Kotakoski. Scientific Reports, **2** 9124, (2019). DOI: 10.1038/s41598-019-49565-4
[54] T. Susi, J.C. Meyer, J. Kotakoski. Nature Rev. Phys., **1**, 397 (2019). DOI: 10.1038/s42254-019-0058-y
[55] O. Dyck, S. Yeom, S. Dillender, A.R. Lupini, M. Yoon, S. Jesse. Carbon, **201**, 212 (2023). DOI: 10.1016/j.carbon.2022.09.006
[56] H. Zhao, N.R. Aluru. J. Appl. Phys., **108**, 064321 (2010). DOI: 10.1063/1.3488620
[57] C.S. Ruiz-Vargas, H.L. Zhuang, P.Y. Huang, A.M. van der Zande, S. Garg, P.L. McEuen, D.A. Muller, R.G. Hennig, J. Park. Nano Lett., **11**, 2259 (2011). DOI:10.1021/nl200429f

Translated by Ego Translating